

Understanding fission fragment mass distributions in a shape modified random neck rupture model

Y. Sawant,* S. V. Suryanarayana, B. K. Nayak, A. Saxena, and R. K. Choudhury
Nuclear Physics Division, Bhabha Atomic Research Centre, Mumbai - 400085, INDIA
(Dated: April 20, 2020)

The variances of the fission fragment mass distributions for symmetric case, over a wide range of the fissility of the compound nucleus have been investigated within the frame work of Random Neck Rupture Model (RNRM) proposed by Brosa et al.. The shape of the fissioning nucleus is generated excluding c_{rel} (i.e. $c_{rel}=1$) in the RNRM model, which results in more continuous shape of fissioning nucleus at boundaries connecting heads to neck in scission shape. This shape modified RNRM model has been used to analyse experimental data of mass variances for symmetric mass distributions of 27 systems in a wide region of fissility 0.7-0.95. The neck radius is an important parameter of the RNRM model and this has been varied to fit the experimental mass variances data. The systematics of resulting neck radii are studied of as a function of fissility and nuclear potential through γ_0 , the surface energy coefficient. Further average total kinetic energies of fission fragments $\langle TKE \rangle$ are studied of as a function of fissility and γ_0 parameter. It is found that the neck radii that fit the experimentally observed variances of the mass distributions fall into two groups and these groups are related to two groups of experimentally observed $\langle TKE \rangle$ s. Empirical formulae have been obtained for the neck radii for these two groups of fissioning systems. Use of the empirical formulae for neck radii predict the mass variances reasonably well for five test systems and it is shown that these empirical neck radii are better estimates than starting with the Rayleigh criterion.

I. INTRODUCTION

Fission fragment mass distribution is an important observable of the fission process that results from shape evolution dynamics of fissioning nucleus. This is in general true for fission induced by any projectile such as neutron, proton, α or heavy ions. It is known that the mass distribution from fission of a fully equilibrated compound system is independent of projectile or entrance channel and depends on the excitation energy and spin of the fissioning nucleus. Studies on the mass distributions provide valuable information about the potential energy landscape of the fissioning nucleus and the complex fission mechanism exhibiting several effects such as symmetric or asymmetric mass distributions, peak to valley ratios, fission fragment angular anisotropy, total fragment kinetic energies, emissions such as neutrons, γ and α during or after scission process known as pre-scission or post-scission multiplicities [1, 2]. These multiplicities and other fission observables are important for understanding the fissioning system shape evolution by means of fission models such as Brosa model or Langevin dynamics.

A large amount of experimental data on the mass distribution in nuclear fission has been generated over the years. Early studies on low-energy fission of actinides revealed the importance of the nuclear shell effects in fission. The main interest in the medium-energy heavy-ion-induced fission is to understand the effects of entrance channel parameters namely, projectile energy,

angular momentum and entrance channel mass asymmetry, on the fission process. An analysis of the data on the variance of the mass distribution over a wide range of the fissility of the compound nucleus was reported in many publications [3–10]. The analysis revealed that the variance of the mass distribution shows fissility (χ) dependence when studied as a function of T_{CN} which represents temperature at the saddle point. However, fissility dependence vanishes when studied as a function of fragment temperature T_F [4], that corresponds to scission point temperature T_{sc} . Thus, the variance of the mass distribution provides important information about the fission process and can be used to test various models of fission such as the saddle point model [11] and the scission point model [12–15]. These models, although qualitatively explain the gross features of the mass distributions, fail to quantitatively explain the mass distributions.

Brosa et al. [15] proposed the random neck rupture model (RNRM) for the calculation of post-fission observables such as mass distribution, kinetic energy distribution and neutron multiplicity. According to this model, the pre-scission shape of the fissioning nucleus dictates the post-fission observables. This model has been successful in explaining the width of the mass distribution in low- as well as medium-energy fission [16]. In the present work, experimentally determined variances of the symmetric mass distributions have been compared with the results from using the modified shape in RNRM for 27 systems, data taken from [4–10, 17–21].

* ysawant@barc.gov.in

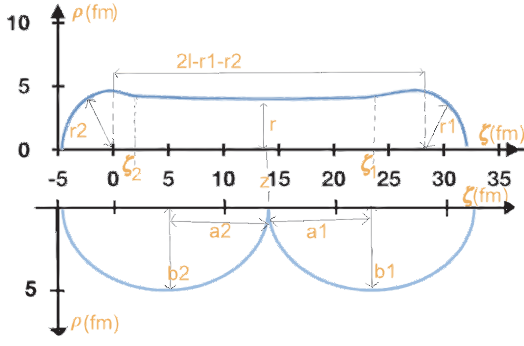


FIG. 1. The shape shown here is a pre-scission shape with flat-neck representation, upper part, and the embedded spheroids, lower part. Lengths are measured in fermi and should be realistic with an accuracy of 10%

II. SHAPE EVOLUTION IN BROSA MODEL

According to Brosa et al. RNRM model [15], the compound nucleus undergoes a shape change from a near spheroidal shape at the saddle point to an elongated deformed shape, called a pre-scission shape, which is the last stage before the neck ruptures. This shape is normally described by a long flat neck connecting two spherical heads. In this model, during the motion of the fissioning nucleus towards scission, a dent is developed in the neck region and is deepened by the capillary force finally leading to fission. The curvature of the fissioning nucleus changes from positive to negative in the motion towards scission. During this transition when the neck becomes flat, there can be a large shift in the position of the dent without sizeable physical mass motion, which finally leads to large mass fluctuations in the fission process. In the RNRM model [15] the pre-scission shape of fissioning nucleus is described by the following set of equations, suitable for symmetric fission.

$$\rho(\zeta) = \begin{cases} \sqrt{r_1^2 - \zeta^2} & -r_1 \leq \zeta \leq \zeta_1 \\ r + a^2 c [\cosh(\frac{\zeta - z}{a}) - 1] & \zeta_1 \leq \zeta \leq \zeta_2 \\ \sqrt{r_1^2 - (2l - 2r_1 - \zeta)^2} & \zeta_2 \leq \zeta \leq 2l - r_1 \end{cases} \quad (1)$$

Equation (1) represents a shape that is made up of two spheres connected by a neck with minimal curvature 'c'. For symmetric case shape made up of two equal spheres can be assumed.

The shape in RNRM model of Eq.(1) is shown schematically in Figure 1. In this work, we consider symmetric fission cases and there are six parameters (r_1 , ζ_1 , r , a , c , l) for this shape. Here, ' r_1 ' is taken as radius of the spherical heads at both ends of the pre-scission shape (for symmetric case, $r_1 = r_2$), ' r ' is the minimal neck radius (r_{neck}) and ζ_1 is the transitional point where

the function describing the shape changes. Also, the position of ζ_2 is calculated using ζ_1 , hence eliminated from parameters list. 'c' is the curvature of the neck, where the neck is thinnest, i.e. at the geometrical centre of the shape in the case of symmetric pre-scission shape. The parameter 'a' is a measure of the extension of the neck and '2l' is the total elongation of the pre-scission shape. By imposing the conditions of continuity of the shape and volume conservation, a set of nonlinear equations were solved to determine r_1 , r , ζ_1 , a and 'c'. Further the parameter 'c' can be correlated to r_1 , r and l using the following equation:

$$c = 2c_{rel} \left(\frac{r_1 - r}{l - r_1} \right) \quad (2)$$

The value of c_{rel} was taken so as to z and dz/dr become continuous at the transitional points z_1 , z_2 as mentioned in [15], which gives continuous shape as well as continuously differentiable shape.

Further we modified shape of Brosa's RNRM model by excluding c_{rel} parameter in curvature formula (i.e. taking $c_{rel} = 1$) resulting in more continuous shape at boundaries connecting heads to neck in scission shape. Remaining variable 'l' was varied to reproduce the experimental average total kinetic energy $\langle TKE \rangle$, taken from Viola systematics [22]. For a given value of l , the pre-scission shape was determined and the probability of neck rupture at different positions of the neck (z_r) was calculated using the following Eq. 3.

$$W(A) = \exp \left(-2\pi\gamma_0 \frac{[\rho^2(z_r) - \rho^2(z)]}{T_{sc}} \right) \quad (3)$$

where,

$$\gamma_0 = 0.9517 \left[1 - 1.7828 \left(\frac{N_{CN} - Z_{CN}}{A_{CN}} \right)^2 \right] \quad (4)$$

In Eq. 4, N_{CN} , Z_{CN} and A_{CN} are the neutron number, atomic number and mass number of the fissioning nucleus and T_{sc} is the temperature of the fissioning nucleus at the scission point. The elongated deformed nucleus at the scission point splits into two deformed fragments and the deformation energy of these nascent fragments gets added to the excitation energy of the fission fragments. This excitation energy is released by evaporation of neutrons from the fragments, which is normally the measure of the temperature of the fragments. The temperature T_{sc} at the scission point was calculated using formula $T_{sc} = \sqrt{E_{sc}^*/a}$, where E_{sc}^* is the excitation energy of the fissioning nucleus at the scission point, ' a ' is level density parameter at scission point. The scission point excitation energy (E_{sc}^*) in terms of fragment's energy (E_{frag}) after scission and deformation energy (E_{def}) at scission point is given by,

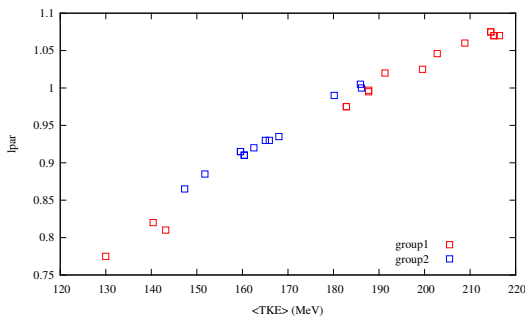


FIG. 2. (Color online) $lpar$ representing scission semilength (l) versus average total kinetic energy of fragments $\langle TKE \rangle$ from Viola systematics [22] from Brosa model calculations.

$E_{sc}^* = (E_{Frag} - E_{def}) A_{CN} / A_{Frag}$. The excitation energy of fragments E_{Frag} after the scission is calculated using formula $E_{Frag} = a^2 T_F$, where T_F is the temperature of the fragment, and 'a' is level density parameter for fragment. The temperature of fragment (T_F) after scission is calculated using method described in Ref. [23].

The random neck rupture produces different mass fragments by chopping the neck at different positions. So one can say that the pre-scission shape is related to the width of mass distribution. More precisely, the variance of the mass distribution strongly depends on the neck of scission point shape. Also, if the temperature at the scission point is high, the fluctuation in the rupture position will be larger and it will give rise to a broader mass distribution. The scission configuration, which includes the scission excitation energy and scission point deformation energy, plays an important role in deciding the width of the mass distribution. The rupture position (z_r) was translated into the fragment mass using the following relation:

$$A(z_r) = \left(\frac{3A_{CN}}{4r_{CN}^3} \right) \int_{-r_1}^{z_r} \rho^2(\zeta) d\zeta \quad (5)$$

As mentioned earlier, we fix $c_{rel} = 1$ and adjust elongation length and neck radius r_{neck} to fit experimental data. The total length of the fissioning shape is maximum about 40fm and we perform shape calculations in step size of 0.02fm in order to smoothly join the heads and neck in the overlapping regions giving a smooth and continuous shape. The average total fragments kinetic energy strongly depends on total elongation length '2l' and here we introduce a parameter $lpar = l / (r_0 * 15)$ fm (with fixed $r_0 = 1.2249$ fm). In the present RNRM calculations, the elongation 'lpar' of the pre-scission shape was varied to reproduce the experimental average total kinetic energy $\langle TKE \rangle$ for given compound nucleus and as well as the shape at scission point. Figure 2 shows typical dependence of $\langle TKE \rangle$ versus these adjusted elongation $lpar$ values. It can be seen that $\langle TKE \rangle$ shows a

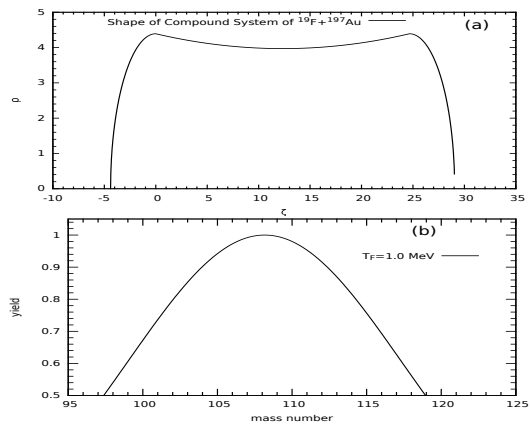


FIG. 3. (Color online) (a) Shape of fissioning compound system formed in $^{19}\text{F} + ^{197}\text{Au}$ using Brosa Model. (b) Fission fragments mass distribution from corresponding shape shown in Fig. 3(a).

linear dependence on elongation (in figure $lpar$ is shown) for all fissioning systems irrespective of entrance channel.

Using this information of scission length for the fissioning nucleus from the experimental $\langle TKE \rangle$ data, the scission point shape of the fissioning nucleus of Brosa's model (as in Figure 1) can be configured for a fixed neck radius r_{neck} and the shape is sensitive to r_{neck} . Further this shape ruptures at different points on flat neck of scissioning nucleus depending on the scission point temperature to produce distribution of fragment masses. The flatness and neck radius influence the width of distribution of fragment masses. Eq. (3) indicates that more the scission point temperature, more will be variance of the mass distribution for given compound nucleus. This shape analyses of the fissioning nuclei were carried out for the 27 systems with real time monitoring of shape configuration using graphic user interface (GUI), while the parameters $lpar$ and r_{neck} were being continuously adjusted for $\langle TKE \rangle$ and mass variances data. In the program, the head radius gets automatically fixed from volume conservation.

As an example of present work, we show in Fig. 3(a) the shape of fissioning compound nucleus formed by $^{19}\text{F} + ^{197}\text{Au}$ system. This shape is attained after adjusting the $lpar$ to fit the $\langle TKE \rangle$ of Viola systematics [22] and also after adjusting the r_{neck} to fit the width of mass distributions data for this system at $T_F = 1.0$ MeV. Once the shape is determined at one temperature, the mass distributions for different temperatures T_F corresponding to respective T_{sc} were calculated using Eq. 3. The resulting mass distribution versus mass number is shown in Fig. 3(b) $T_F = 1.0$ MeV and the intercepts on x-axis give full width at half maximum (maximum is 1.0) for the mass distribution and using this the variance can be calculated.

TABLE I. r_{neck} , γ_0 , χ , $lpar$ for different systems in two groups

System-group1	γ_0	χ	$lpar$	r_{neck}	Ref.
$^{16}\text{O}+^{209}\text{Bi}$	0.88974	0.77376	0.935	3.9	[5]
$^{12}\text{C}+^{232}\text{Th}$	0.87465	0.80778	0.99	4.008	[5]
$^{16}\text{O}+^{232}\text{Th}$	0.87711	0.82588	1.005	4.0205	[5]
$^{16}\text{O}+^{204}\text{Pb}$	0.89562	0.76897	0.93	3.97	[9]
$^{16}\text{O}+^{208}\text{Pb}$	0.88624	0.76323	0.93	4.0086	[9]
$^{30}\text{Si}+^{186}\text{W}$	0.89352	0.75055	0.91	3.97	[8]
$^{19}\text{F}+^{197}\text{Au}$	0.89352	0.75055	0.91	3.97	[8]
$^{12}\text{C}+^{204}\text{Pb}$	0.89352	0.75055	0.91	3.97	[8]
$^4\text{He}+^{209}\text{Bi}$	0.88256	0.71893	0.885	3.9924	[10]
$^4\text{He}+^{201}\text{Tl}$	0.8903	0.70605	0.865	3.9925	[10]
$^{12}\text{C}+^{209}\text{Bi}$	0.88748	0.75544	0.92	4.0082	[4]
$^{12}\text{C}+^{235}\text{U}$	0.87937	0.82709	1	4.0315	[4]
$^{12}\text{C}+^{208}\text{Pb}$	0.88384	0.74497	0.915	3.965	[4]
$^{11}\text{B}+^{209}\text{Bi}$	0.88384	0.74497	0.915	3.965	[4]
$^{48}\text{Ca}+^{208}\text{Pb}$	0.8983	0.87357	1.025	4.02	[20]
System-group2	γ_0	χ	$lpar$	r_{neck}	Ref.
$^{238}\text{U}+^{16}\text{O}$	0.87502	0.84163	1.02	4.12	[7]
$^{238}\text{U}+^{26}\text{Mg}$	0.87537	0.87548	1.046	4.127	[7]
$^{32}\text{S}+^{208}\text{Pb}$	0.89468	0.83665	0.997	4.0413	[6]
$^{26}\text{Mg}+^{248}\text{Cm}$	0.87568	0.90933	1.075	4.1	[19]
$^{36}\text{S}+^{238}\text{U}$	0.87568	0.90933	1.075	4.1	[19]
$^{22}\text{Ne}+^{249}\text{Cf}$	0.88182	0.913	1.07	4.0925	[19]
$^{58}\text{Fe}+^{208}\text{Pb}$	0.89176	0.91979	1.07	4.095	[19]
$^{40}\text{Ca}+^{192}\text{Os}$	0.90127	0.82446	0.975	4.0442	[18]
$^{40}\text{Ca}+^{142}\text{Nd}$	0.92692	0.70964	0.81	3.95	[18]
$^{13}\text{C}+^{176}\text{Yb}$	0.88668	0.64472	0.775	4.0354	[17]
$^{13}\text{C}+^{182}\text{W}$	0.89705	0.68439	0.82	4.0262	[17]
$^{30}\text{Si}+^{238}\text{U}$	0.87763	0.89359	1.06	4.15	[21]

Table 1 shows the list of systems of symmetric fission cases studied, the γ_0 and (χ) parameters of the compound systems, the $lpar$ values that fit $\langle\text{TKE}\rangle$ data, r_{neck} that fit the experimental variances data and references. The experimental mass variances are very well reproduced by varying neck radii of scission shape within modified shape of Brosa's RNRM model and the best fit values are shown in column 5 of the Table. 1. The detailed study of effect of various parameters such as fissility (χ), average total kinetic energy of fission fragments $\langle\text{TKE}\rangle$ through $lpar$, nuclear potential through, γ_0 (surface energy coefficient) parameter and entrance channel, on the neck radius (r_{neck}), is discussed below.

III. SYSTEMATICS OF VARIOUS PARAMETERS OF BROSA MODEL

As mentioned before, to reproduce experimental mass variances [4–10, 17–21], the neck radii (r_{neck}) have been adjusted. The resulting r_{neck} values have been analysed as a function of fissility, γ_0 and other parameters. The fitted r_{neck} values do not show any systematic behaviour. However, it is observed that the quantity ($r_{neck} - 2 * lpar$) versus fissility (χ) shows very good systematic trend and this quantity falls into two groups as a function of

(χ), as shown in Fig. 4(a). The two groups in Fig. 4(a) with blue and pink symbols, can be fitted with equation of the form $(k+m/\chi^2)$ with two values of constant k ($=1.33, 1.41$) with same $m=0.46$ value as shown by blue and pink coloured lines.

The empirical formulae in Fig. 4(a) give ($r_{neck} - 2 * lpar$) values and from these the r_{neck} values can be obtained by adding $2 * lpar$. These empirically determined neck radii are shown in Fig. 4(b) by pink symbols along with r_{neck} values of Table. 1 in blue symbols. It can be seen from Fig. 4(b), the empirical r_{neck} values are very close to r_{neck} values of Table. 1. The percentage variation of empirical r_{neck} from r_{neck} values of Table. 1 are shown in Fig. 4(c). The variation is within $\pm 0.5\%$, which can introduce

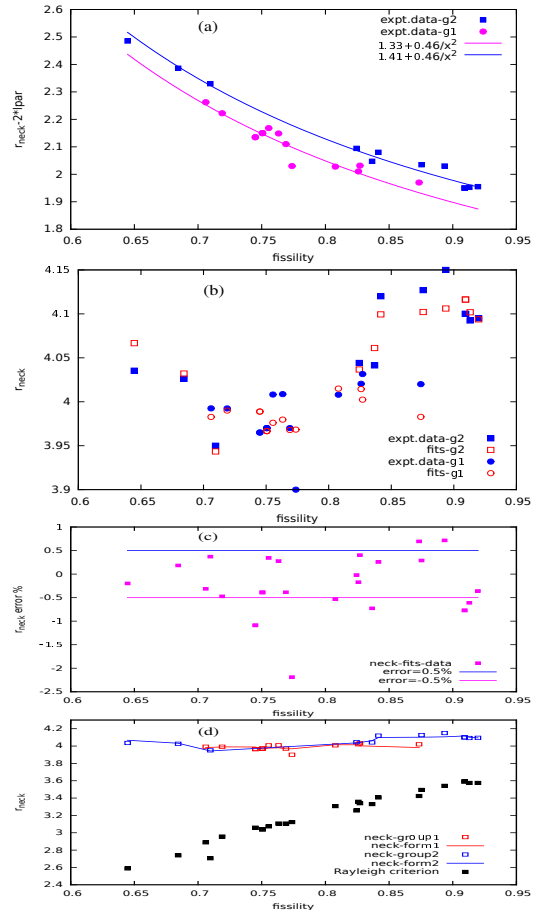


FIG. 4. (Color online) (a) variable ($r_{neck} - 2 * lpar$) vs fissility (χ) with empirical fits for two groups in blue and pink colour. (b) r_{neck} vs (χ) with blue colour for neck radii from Table 1 column 5 and pink colour for radii obtained using fitted parameters of Fig. 4(a). (c) r_{neck} error in % vs (χ). Straight lines are limits for $+0.5\%$ error (blue) and -0.5% error (pink) in radii for fitted Eqns. (d) Variation in r_{neck} from empirical values (lines) and data from Table 1. (symbols), as a function of (χ) as compared to r_{neck} values from Rayleigh criterion (filled black square) [15].

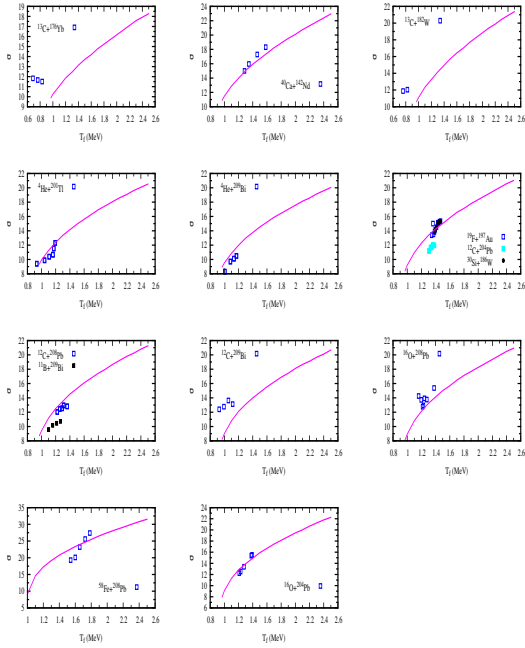


FIG. 5. (Color online) (a) mass variances versus T_F using shape modified RNRM using two empirical formulae for neck size, as discussed in Fig. 4.

error upto 2 mass units in standard deviation of fission fragment mass distribution. The r_{neck} values from Rayleigh criterion, suggested in [15] are compared with empirical r_{neck} values as shown in Fig. 4(d). It can be seen that empirical r_{neck} values obtained from any of two fits formulae are better estimates than starting with the Rayleigh criterion.

Using the systematics study and the empirical formulae for neck radii, we recalculated mass variances values for all the 27 systems for all temperatures using RNRM model. Figures 5(a,b) show the experimental fission fragment mass variances data as a function of temperature of fragment T_F along with lines predicted using empirical r_{neck} (from equations in figure 4(a)). All systems show reasonable agreement with predictions using shape modified Brosa model. However, the two systems $^{13}\text{C} + ^{182}\text{W} \rightarrow ^{195}\text{Hg}$ and $^{13}\text{C} + ^{176}\text{Yb} \rightarrow ^{189}\text{Os}$ show large deviations, may be due to shell effects as mentioned in [17] resulting in asymmetric fission. So, these data of the two systems cannot be analysed with this shape model which is mainly suitable for symmetric fission.

As mentioned before, the experimental $\langle \text{TKE} \rangle$ values of Viola systematics [22] have been reproduced by adjusting $lpar$ value in Brosa model and these $lpar$ versus fissility are shown in Fig. 6(a). As seen in figure, $lpar$ values exhibit two groups, whereas no systematic behaviour was found with respect to either fissility or γ_0 . However, when $(lpar * \gamma_0)$ is

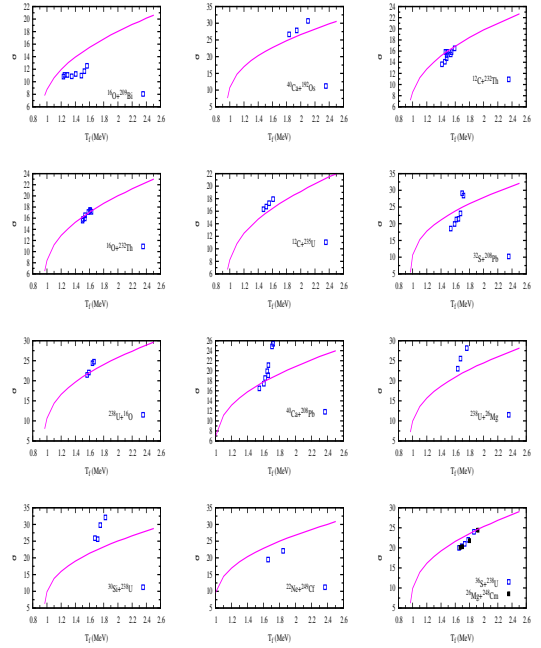


FIG. 5. (Color online) (b) mass variances versus T_F obtained similar to Fig. 5(a).

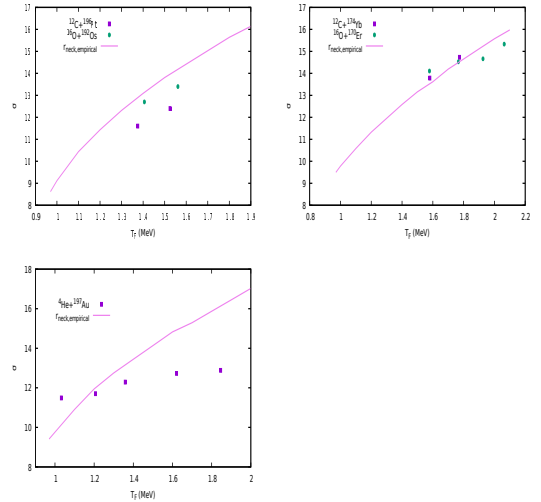


FIG. 5. (Color online) (c) mass variances versus T_F using shape modified RNRM using two empirical formulae for neck size, as discussed in Fig. 4(a). and selection of value of 'k' parameter using grouping shown in Fig. 6(b) for five test systems from Refs.[24, 25], below to show predictive power of two-fit formula.

plotted versus fissility, these two groups clearly separate from each other, as shown in Fig. 6(b). This effect is also observed in r_{neck} as discussed in Fig. 4(a). This indicates nuclear potential plays important role through γ_0 affecting mass variances of fissioning systems.

To verify the validity of empirical systematic formulae, studied in present work, we have applied those formulae

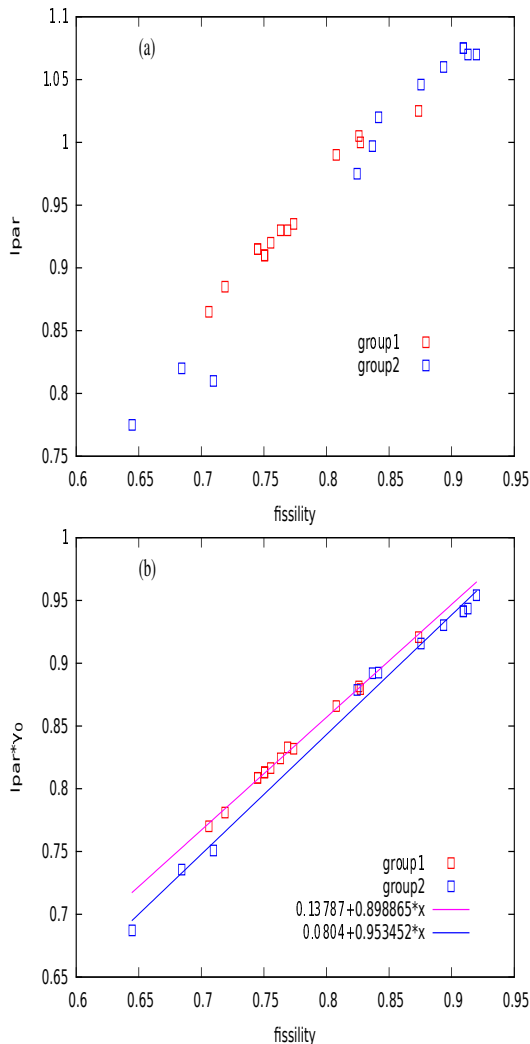


FIG. 6. (Color online) (a) $lpar$ vs fissility and (b) $lpar * \gamma_0$ vs fissility.

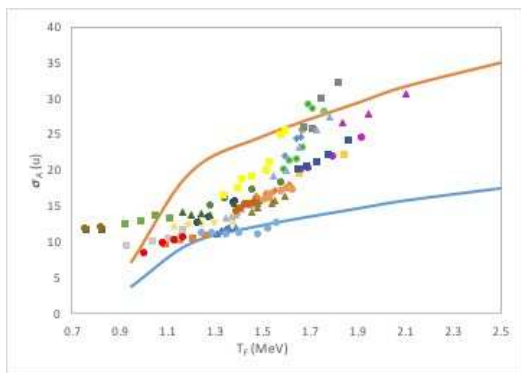


FIG. 7. Symbols shows Exp. data [4–10, 17–21] whereas lines for shape modified Brosa model calculations set up. The experimental uncertainties are within the symbol sizes.

to experimental mass variance data of five additional systems from Refs.[24, 25]. The comparison of experimental mass distributions with theoretically predicted values of mass distributions are shown in Fig. 5(c) by lines. It can be seen from Fig. 5(c), the experimentally observed width of fission fragments mass distribution is very well reproduced by using r_{neck} obtained by two-fits formulae. The value of coefficient 'k' in the two-fits formulae is chosen using grouping shown in $(lpar * \gamma_0)$ vs fissility, plot in Fig. 6(a). Thus, the predictive power of empirical systematic formulae in present study, can be clearly seen from Fig. 5(c).

Figure 7 shows mass variances for all systems studied collectively, as a function of fragment temperature (T_F). The calculations were carried out using shape modified RNRM Brosa Model and are shown by two theoretical lines. In the calculation, for each T_F , the r_{neck} values are varied from mean $\langle r_{neck} \rangle$ values by $\pm 2.9\%$, to obtain range of mass variances values shown by two theoretical lines in Fig. 7. The mean $\langle r_{neck} \rangle$ value is taken that of $^{12}\text{C}+^{235}\text{U}$ system and the mass distributions calculated for same system by varying $\langle r_{neck} \rangle$ values by $\pm 2.9\%$, as shown by lines in Fig. 7. The change in r_{neck} values change in flatness of neck and thus controls mass distributions. In Fig. 7, symbols shows experimental data [4–10, 17–21], whereas lines are results of shape modified RNRM calculations. The experimental uncertainties are within the symbol sizes.

IV. CONCLUSION

The variances of the fission fragment mass distributions for symmetric fission over a wide range of the fissility of the compound nucleus have been studied by modifying shape of the Random Neck Rupture Model (RNRM) of Brosa et al., by excluding the parameter c_{rel} in curvature formula (i.e. taking $c_{rel} = 1$). This shape modified RNRM model has been used to analyse experimental data of mass variances for symmetric mass distributions of 27 systems covering a wide region of fissility 0.7–0.95. The average total kinetic energies of fission fragments $\langle TKE \rangle$ have been fitted by adjusting the elongation ($lpar$ values) of the fissioning nucleus shape. The neck radius (r_{neck}) of the RNRM model has been varied to fit the experimental mass variances data. The systematics of the fitted $lpar$ and r_{neck} values are studied of as a function of fissility and nuclear potential through, γ_0 parameter. It is observed that the r_{neck} values fall into two groups and these groups are related to two groups of experimentally observed $\langle TKE \rangle$ s. Empirical formulae have been obtained for the r_{neck} of these two groups of the fissioning systems. The five more test systems have been used for validating systematics approach as shown in Fig. 4(a) and Fig. 6(b) of present work. The grouping systematic shown in Fig. 6(b) helps in selecting one equation out of two equations of two-fits empirical for-

mulae for r_{neck} . which produces mass variances which agrees reasonably well with experimental mass variances

of five test systems. Overall study shows that these empirical neck radii are better estimates than starting with the Rayleigh criterion.

-
- [1] R. Vandenbosch and J. Huizenga, *Nuclear Fission* (Academic Press, Inc., New York, 1973).
- [2] C. Waggemans, *The Nuclear Fission Process* (CRC, London, 1991).
- [3] A. Rusanov, M. Itkis, and V. Okolovich, *Z. Phys* **A342**, 299 (1997).
- [4] Y. Sawant, A. Saxena, R. K. Choudhury, B. K. Nayak, L. M. Pant, and et al., *Phys. Rev.* **C 70**, 051602 (2004).
- [5] R. K. Choudhury, A. Saxena, A. Chatterjee, D. V. Shetty, and S. S. Kapoor, *Phys. Rev.* **C 60**, 054609 (1999).
- [6] N. P. Shaw and et al., *Phys. Rev.* **C 61**, 044612 (2000).
- [7] W. Q. Shen and et al., *Phys. Rev.* **C 36**, 115 (1987).
- [8] A. C. Berriman, D. J. Hinde, M. Dasgupta, C. R. Morton, R. D. Butt, and J. O. Newton, *Nature (London)* **413**, 144 (2001).
- [9] G. G. Chubarian and et al., in *Proceedings of the 4th International Conference on Dynamical Aspects of Nuclear Fission (DANF'98)* (World Scientific, Singapore, 2000) p. 293.
- [10] S. V. Zhdanov, M. G. Itkis, S. I. Mulgin, V. N. Okolovich, and et al., *Sov. J. Nucl. Phys.* **55**, 1766 (1992).
- [11] J. R. Nix and W. J. Swiatecki, *Nucl. Phys.* **71**, 1 (1965).
- [12] C. Tsang and J. Wilhelmy, *Nucl. Phys.* **A 184**, 417 (1972).
- [13] B. Wilkins, E. Steinberg, and R. Chasman, *Phys. Rev.* **C 14**, 1832 (1976).
- [14] U. Brosa and S. Grossmann, *Phys. Lett.* **B 126**, 425 (1983).
- [15] U. Brosa, S. Grossmann, and A. Muller, *Phys. Rep.* **197**, 167 (1990).
- [16] U. Brosa, *Phys. Rev.* **C 32**, 1438 (1985).
- [17] K. Ramachandran and et al., *EPJ Web of Conf.* **63**, 02017 (2013).
- [18] E. Prasad and et al., *Phys. Rev.* **C 96**, 034608 (2017).
- [19] I. M. Itkis and et al., *Phys. Rev.* **C 83**, 064613 (2011).
- [20] E. V. Prokhorova and et al., *Nucl. Phys.* **A 802**, 45 (2004).
- [21] K. Nishio and et al., *Phys. Rev.* **C 82**, 044604 (2010).
- [22] V. E. Viola, K. Kwiatkowski, and M. Walker, *Phys. Rev.* **C 31**, 1550 (1985).
- [23] A. Saxena, A. Chatterjee, R. K. Choudhury, S. S. Kapoor, and D. M. Nadkarni, *Phys. Rev.* **C 49**, 932 (1994).
- [24] Cuninghame and et al., in *Proc. IAEA Symp. Physics and Chemistry of Fission, (Jlich 1979)*, Vol. I (IAEA, Vienna, 1980) p. 551.
- [25] F. Plasil and et al., *Phys. Rev.* **142**, 696 (1966).